IV International Conference on Computational Methods for Coupled Problems in Science and Engineering
COUPLED PROBLEMS 2011
M. Papadrakakis, E. Oñate and B. Schrefler (Eds)

INVESTIGATION OF THE PURELY HYPERBOLIC MAXWELL SYSTEM FOR DIVERGENCE CLEANING IN DISCONTINUOUS GALERKIN BASED PARTICLE-IN-CELL METHODS

Andreas Stock*, Jonathan Neudorfer†, Rudolf Schneider ‡, Christoph Altmann† and Claus-Dieter Munz†

* †Institute for Aerodynamics and Gasdynamics (IAG)
University of Stuttgart
Pfaffenwaldring 21, 70569 Stuttgart, Germany
e-mail: stock@iag.uni-stuttgart.de, www.iag.uni-stuttgart.de

‡Karlsruhe Institute of Technology
Institute for Pulsed Power and Microwave Technology,
PF 3640, 76021 Karlsruhe, Germany
e-mail: rudolf.schneider@kit.edu, www.ihm.kit.edu

Key words: Particle-In-Cell (PIC) Method, Computational Plasma Physics, Hyperbolic Divergence Cleaning, Discontinuous Galerkin (DG) Method

Abstract. For the Particle-In-Cell (PIC) method which is used to simulate non-neutral plasma the charge conservation is violated. To solve this problem several approaches have been suggested. In this paper we shall investigate the hyperbolic divergence cleaning method. It has been proposed in two different manners, one enforcing only Gauss' law and another considering both Gauss' law and the magnetic monopole divergence constraint. We shall investigate the differences between the two approaches with numerical simulations of a quasi 2D diode with the PIC method and a pure Maxwell equations example satisfying the charge conservation in its initial conditions. We use a discontinuous Galerkin FEM-type space discretization method to solve the Maxwell equations. The results of the numerical investigations are presented and the advantages or disadvantages of both approaches w.r.t. performance and quality are discussed.

1 Introduction

For given charge and current density, ρ and $\mathbf{j}$, the evolution of the electromagnetic field is given by the Maxwell equations,

$$\frac{\partial \mathbf{E}}{\partial t} = c^2 \nabla \times \mathbf{B} - \frac{\mathbf{j}}{\varepsilon_0}, \tag{1}$$

$$\frac{\partial \mathbf{B}}{\partial t} = -\nabla \times \mathbf{E}, \tag{2}$$

$$\nabla \cdot \mathbf{B} = 0, \tag{3}$$

$$\nabla \cdot \mathbf{E} = \frac{\rho}{\varepsilon_0}, \tag{4}$$

where $\mathbf{E}$ and $\mathbf{B}$ denote the electric field and the magnetic induction field, respectively. c is the speed of light and ε_0 is the electric permittivity.

When ρ and $\mathbf{j}$ satisfy the charge conservation equation

$$\frac{\partial \rho}{\partial t} + \nabla \cdot \mathbf{j} = 0, \tag{5}$$

for all times $t \geq 0$, and when the initial $\mathbf{E}$ and $\mathbf{B}$ satisfy (4) and (3), respectively, the Maxwell system of hyperbolic evolution equations (1) and (2) has a unique solution.

In the discrete case, i.e. using a numerical method such as the Finite-Element or Finite-Volume method, approximation errors of the fields $(\mathbf{E}, \mathbf{B})$ and the sources $(\rho, \mathbf{j})$ lead to small inconsistencies accumulating to large errors for long simulation times. Thus, the charge conservation (5) is not satisfied by the discrete approximation any more. In the scope of the Maxwell equations this means that Gauss' law (4) is violated.

Another situation where the charge conservation is not satisfied occurs in the Particle-In-Cell (PIC) framework where particles and fields are simulated in a self-consistent manner on discrete level [3, 4, 9]. In the PIC technique the particles are directly used as sources that are assigned to the grid via special deposition methods, e.g. nearest-grid-point, volume-weighting or shape-function [3, 9]. The deposition leads to errors in Gauss' law (4) which can become very large in the course of time.

To resolve this problem mainly two approaches have been proposed, i.e. the projection method [3] and a set of methods relying on a generalized Lagrange multiplier (GLM) approach for the Maxwell equations. The latter has three different formulations, the hyperbolic-elliptic constrained formulation proposed by Assous et al. [2], the hyperbolic-parabolic form introduced by Marder [11] and the purely hyperbolic Maxwell (PHM) system introduced by Munz et al. [12, 13], known as hyperbolic divergence cleaning.

In the frame of the standard projection approach a Poisson equation has to be solved which requires large computational effort and is cumbersome for straightforward implementation of the scheme on parallel platforms.

The hyperbolic divergence cleaning technique seemed to be the best choice w.r.t. numerical complexity, locality and parallelization since it can be solved explicitly and, beyond that, yields qualitatively similar results to the projection method [9]. It is easy to

implement in an explicit discontinuous Galerkin method, which will be used within this work.

To satisfy charge conservation (5) the divergence constraint of Gauss' law (4) has to be coupled with the evolution equation (1). This is done by a generalized Lagrange multiplier Φ. For the hyperbolic divergence cleaning Munz et al. proposed in [12] to incorporate the Lagrange multiplier in the Maxwell equations as follows

$$\frac{\partial \mathbf{E}}{\partial t} = c^2 \nabla \times \mathbf{B} - c^2 \nabla \Phi - \frac{\mathbf{j}}{\varepsilon_0}, \tag{6a}$$

$$\frac{\partial \mathbf{B}}{\partial t} = -\nabla \times \mathbf{E}, \tag{6b}$$

$$\frac{\partial \Phi}{\partial t} = -\chi^2 \nabla \cdot \mathbf{E} + \chi^2 \frac{\rho}{\varepsilon_0}, \tag{6c}$$

where χ is a positive dimensionless parameter. The new variable Φ is an additional degree of freedom, leading to a seven variable system in three space dimensions, named PHM7 in the following. The physical interpretation of the new variable is a correction potential that transports the divergence errors of the electrical field out of the domain with the speed $\chi \cdot c$. The higher χ is the better (4) is satisfied. Obviously the monopole constraint (3) for the magnetic fields is left out of consideration in the PHM7 system. None the less it was recognized that violations of the magnetic divergence constraint also appear, similar as in the context of Magneto-Hydro-Dynamics (MHD) [5, 1]. Thus in the same year Munz et al. presented in [13] a system involving the magnetic divergence constraint, yielding

$$\frac{\partial \mathbf{E}}{\partial t} = c^2 \nabla \times \mathbf{B} - \chi c^2 \nabla \Phi - \frac{\mathbf{j}}{\varepsilon_0}, \tag{7a}$$

$$\frac{\partial \mathbf{B}}{\partial t} = -\nabla \times \mathbf{E} - \gamma \nabla \psi, \tag{7b}$$

$$\frac{\partial \Psi}{\partial t} = -\gamma c^2 \nabla \cdot \mathbf{B}, \tag{7c}$$

$$\frac{\partial \Phi}{\partial t} = -\chi \nabla \cdot \mathbf{E} + \chi \frac{\rho}{\varepsilon_0}, \tag{7d}$$

where γ has the same function as χ. This system couples the originally elliptic divergence constraint (3) with the hyperbolic evolution equation (2) through the additional variable Ψ, yielding eight variables in total. Thus we call it PHM8 in the following. In this paper we shall investigate the differences between the PHM7 and PHM8 system w.r.t. the quality of the divergence cleaning and the performance with the help of a pure Maxwell equation and a PIC problem.

1.1 Numerical Method

For the spatial discretization we use a mixed nodal and modal FEM-type discontinuous Galerkin (DG) method [6, 7] and a low storage fourth-order explicit Runge-Kutta (LSERK4) scheme [10] for the temporal time discretization.

The computational domain Ω is divided into K non-overlapping hexahedral or tetrahedral elements; pyramids and prisms are also possible. In each element locally the state vector $\mathbf{u}^k(\mathbf{x},t)$ is approximated by a polynomial $\mathbf{u}_h^k(\mathbf{x},t)$ of order p,

$$\mathbf{u}^k(\mathbf{x},t) \approx \mathbf{u}_h^k(\mathbf{x},t) = \sum_{i=1}^{M} \tilde{\mathbf{u}}^k(\mathbf{x}_i,t) L_i(\mathbf{x}) = \sum_{n=1}^{N} \hat{\mathbf{u}}_n^k(t) \phi_n(\mathbf{x}) \tag{8}$$

where $\{L_i\}_{i=1,\dots,M}$ is the multivariate Lagrange basis, $\tilde{\mathbf{u}}(\mathbf{x}_i,t)$ is the state evaluated at M nodal interpolation points (IPs) $\mathbf{x}_i$, $\{\phi_n\}_{n=1,\dots,N}$ is the modal basis and $\hat{\mathbf{u}}(t)$ the modal coefficients. In three dimensions each element needs $N = (p+1)(p+2)(p+3)/6$ modal degrees of freedom (DOF). The choice of M and the location of the IPs $\mathbf{x}_i$ is discussed in [6]. M only equals N in case of linear tetrahedrons; for all other types of elements $M > N$. Important for the spatial resolution of the electromagnetic fields is the number of IPs in different element types. This has to be taken into account later when comparing the Cartesian mesh build with hexahedral elements and the unstructured mesh build with tetrahedral elements. The modal polynomial is used to achieve a quadrature free method and the nodal polynomial is used to determine the physical fluxes as well as to incorporate the sources, i.e. the particles in the PIC method. For further details on the DG method we refer to [7].

2 Numerical Experiments

In order to quantify errors arising from the approximation of the magnetic divergence constraint (3) and Gauss' law (4), mainly two quantities will be investigated: The divergence of the magnetic field component, $\nabla \cdot \mathbf{B}$, and the error in Gauss' law, $\nabla \cdot \mathbf{E} - \rho/\varepsilon_0$, which indirectly also measures the violation of the charge conservation (5). We consider the L_2-norm of the time derivative of the Lagrange multiplier. For instance, in the case of the PHM8 system we obtain

$$\frac{1}{\chi} \| \frac{\partial \Phi}{\partial t} \|_{L_2} := \frac{1}{\chi} \sqrt{\int_\Omega \left| \frac{\partial \Phi}{\partial t} \right|^2 dV} = \sqrt{\int_\Omega \left| \nabla \cdot \mathbf{E} - \frac{\rho}{\varepsilon_0} \right|^2 dV}. \tag{9}$$

Here we evaluate the right expression because in this case, even for $\chi = 0$, the norm can be computed. In the following we will call (9) the divergence error of the charge conservation. The L_2-norm of the magnetic field divergence is computed in a similarly straightforward way.

For the PHM8 system we always set $\chi = \gamma$. A different value can be chosen if it is necessary to clean the divergence of one of the two electromagnetic field components stronger than the other.

2.1 Example - 3D Issautier Example

The following example points out the significant differences between the PHM8 and PHM7 systems. In PIC codes the charge conservation (5) usually is violated due to the deposition method. In a pure Maxwell equation setup without particles but analytically

initiated sources we can force charge conservation. This has been done by Issautier et al. for a two-dimensional transverse electric (TE) Maxwell system [8]. We extended their idea to a three-dimensional fully electromagnetic setup with the sources

$$\rho(\mathbf{x},t) = \sin(\omega t)\left[\sin(\pi y)+\sin(\pi x)+\sin(\pi z)\right],$$
$$j_x(\mathbf{x},t) = (\cos(\omega t)-1)\left[\pi\cos(\pi x)+\pi^2 x\sin(\pi z)\right]-\cos(\omega t)x\sin(\pi z), \tag{10a}$$
$$j_y(\mathbf{x},t) = (\cos(\omega t)-1)\left[\pi\cos(\pi y)+\pi^2 y\sin(\pi x)\right]-\cos(\omega t)y\sin(\pi x), \tag{10b}$$
$$j_z(\mathbf{x},t) = (\cos(\omega t)-1)\left[\pi\cos(\pi z)+\pi^2 z\sin(\pi y)\right]-\cos(\omega t)z\sin(\pi y). \tag{10c}$$

The divergence of the current density is

$$\nabla\cdot\mathbf{j} = -\cos(\omega t)\left[\sin(\pi y)+\sin(\pi x)+\sin(\pi z)\right], \tag{11}$$

and the derivative of the charge density yields

$$\frac{\partial\rho}{\partial t} = \cos(\omega t)\left[\sin(\pi y)+\sin(\pi x)+\sin(\pi z)\right], \tag{12}$$

satisfying the charge conservation equation (5). The spatial setup is given as a unity cube by $(1\times1\times1\ [\mathrm{m}^3])$ centered in the origin with irradiation boundaries (see [12]) and $\omega = 10^{-9}$ [1/s]. For the Cartesian mesh we used $10\times10\times10$ hexahedrons and for the unstructured mesh roughly 2400 tetrahedrons. Note that a hexahedron can be filled with six tetrahedrons of the same edge length. The edge length does not necessarily determine the resolution since in our DG implementation a fourth-order hexahedron has 56 IPs and a tetrahedron has 20 IPs, yielding 56000 IPs and 48000 IPs for the Cartesian unstructured mesh, respectively. Therefore we can assume a nearly equal resolution even if the number of tetrahedrons does not multiply by a factor of six.

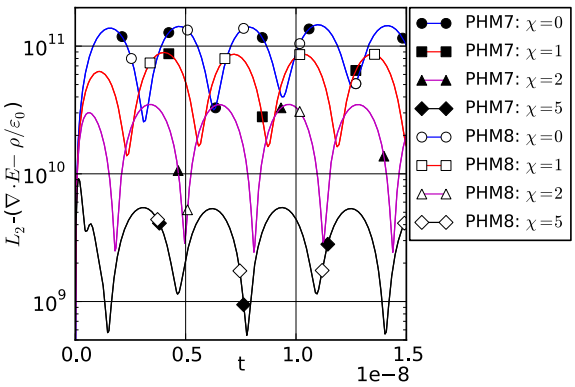

Figure 1: L_2-norm of charge conservation error for the Cartesian mesh.

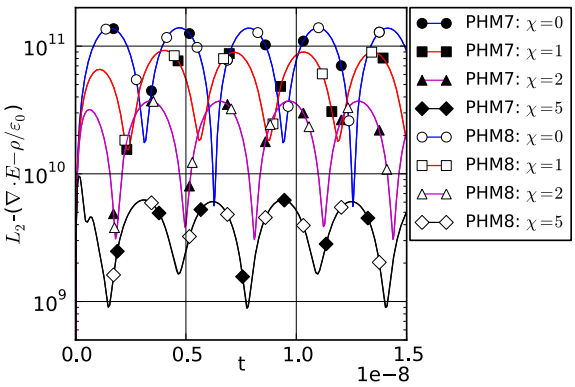

Figure 2: L_2-norm of charge conservation error for the unstructured mesh.

The computations have been performed with $\chi = [0,1,2,5]$ and a fourth-order DG method. Figure 1 and 2 show the L_2-norm (9) for the Cartesian and the unstructured mesh computed with the PHM system. The results of both PHM systems are equal.

There is no difference between the PHM7 and PHM8 results. This is reasonable since the compared L_2-norm (9) is based in both cases on the same equations, i.e. (1) and (4) with the specific Lagrange multiplier Φ. The influence of the magnetic field component in this early phase of the simulation is still small enough and does not influence the electric field. In a later phase when the magnetic field component is stronger developed it will also affect the electrical field and a difference between the PHM7 and PHM8 system will occur. In good comparison with results by [12, 13] the error is damped more strongly with increasing χ.

Not very well visible, the Cartesian mesh evolves slightly lower errors than the unstructured mesh, especially for $\chi = 5$. It is known that unstructured grids evolve higher divergence errors [12, 13]. None the less, an optimal mesh requires a detailed analysis of the wave propagation directions. A spherical structured mesh might be an even better choice for this problem.

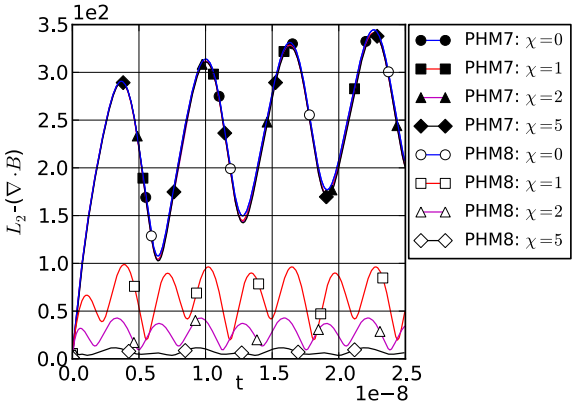

Figure 3: L_2-norm of $\nabla \cdot \mathbf{B}$ for the Cartesian mesh.

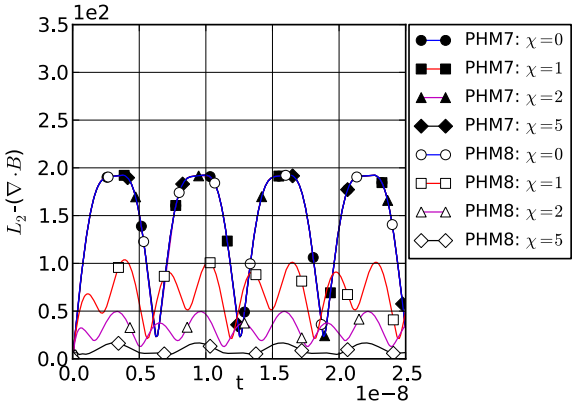

Figure 4: L_2-norm of $\nabla \cdot \mathbf{B}$ for the unstructured mesh.

Figure 3 and 4 show the divergence of the magnetic field for the Cartesian and the unstructured mesh. With the PHM7 system and the Cartesian mesh, with any χ the magnetic divergence is equal and growing. For the unstructured mesh it is continuously oscillating without increase. In both cases the divergence of the magnetic field is much larger than for the PHM8 system. This is obvious since (3) is not enforced by the PHM7 system. In contrast to that, for the PHM8 system with $\chi = \gamma = [1, 2, 5]$ the divergence is damped to a lower and not growing value. For the PHM8 system with $\chi = \gamma = 0$ the divergence evolves equal to the PHM7 system since the constraint (3) is not enforced either. In agreement to the previous results for the charge conservation, also the Cartesian mesh shows better results for the damping of the magnetic divergence.

The influence of the magnetic field on the electric field is described by (1). There it is added with the factor c^2 to the derivative of the electric field. Thus, even a small divergence error in the magnetic fields affects the electric field. The growing values of the magnetic divergence for the PHM7 system with the structured mesh and also the non-

growing values for the unstructured mesh might become a problem for longer simulation times because the Poynting vector $\sim \mathbf{E} \times \mathbf{B}$ becomes erroneous. These results clearly demonstrate the necessity of enforcing also the magnetic divergence constraint, as in the PHM8 system.

Concerning the computational performance the expectation is that the PHM7 system is faster than the PHM8 system since one variable less has to be computed. In an optimal sense this would mean a reduction of the computational time of 12.5 %. Of course this is not realistic since a certain overhead (data-structure, I/O, initialization, etc.) exists. None the less a significant reduction of about 5 to 10 % can be expected.

Table 1 lists up the computational time t_{Tot} for this example. The initialization time is below 1 % of t_{Tot} to guarantee that mainly the performance of the DG scheme is measured. The speed-up S is given as $1 - t_{Tot,PHM7}/t_{Tot,PHM8}$.

Contrary to the expectation it seems as if the PHM7 system is slower than the PHM8 system. In total, we performed 11 runs leading to a mean value of -0.025 for the speed up and a relatively large standard deviation of 0.032, which means that in some runs we also achieved a positive speed up. Obviously for this test case the PHM7 system is even slower than the PHM8 system. None the less, w.r.t. the standard deviation we can identify a certain scattering of the results, which lies within the range of scattering that arises by performing the same computation again and again.

For the memory consumption we found a reduction of ≈ 1.5 % for the PHM7 system.

	$\chi = 0$		$\chi = 1$		$\chi = 2$		$\chi = 5$	
	PHM7	PHM8	PHM7	PHM8	PHM7	PHM8	PHM7	PHM8
t_{Tot} [s]	792.38	753.82	3111.71	3101.47	1492.81	1524.40	3840.32	3824.26
S [−]	-0.051		-0.003		0.021		-0.004	

Table 1: Computational time t_{Tot} and speed-up S for the Issautier example with different χ. Note, that the simulation time for each run was different.

2.2 Example - 2D Diode

To show the impact of the hyperbolic divergence cleaning, we chose a simple but very typical situation occurring in the context of PIC simulations. The domain ($0.1 \times 0.1 \times 0.0015$ [m^3]) is considered to be a plane diode with cathode and anode situated on the left and on the right sides, respectively. Figures 5 and 6 show the domain in the x-y-plane for a Cartesian and an unstructured mesh which have been used in the following computations. The spatial setup is a three-dimensional grid trying to imitate a plane two-dimensional diode. In x-direction we have implemented perfectly conducting, in y-direction open and in z-direction periodic boundaries.

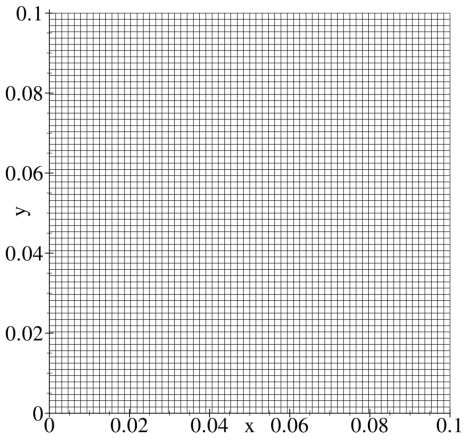

Figure 5: Cartesian grid of $64 \times 64 \times 1$ second-order hexahedrons with ≈ 33000 IPs.

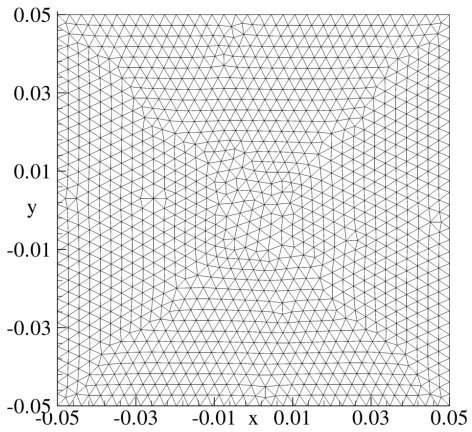

Figure 6: Unstructured grid of 7452 second-order tetrahedrons (edge length 0.0001) with $\approx$ 30000 IPs.

In the center of the cathode we inject an electron beam imitating a current density that has 75% of the space charge limiting current density. The length of the emitter is 37.5 [mm], the voltage is 100 [kV] and the current density is ≈ 5536 [Am^{-2}]. The current density is simulated by an electron beam where 9000 charges/ns are injected with a macro particle factor[1] of $2.180367 \cdot 10^5$, which are accelerated in x-direction by an external electric field of -10^6 [Vm^{-1}]. In the following we will only consider the PHM8 system since no significant qualitative and quantitative differences compared to the PHM7 system have been found.

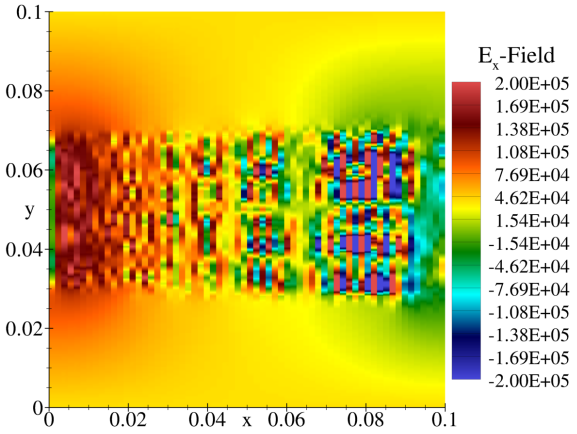

Figure 7: E_x-field at 50 [ns] of y-x-plane slice at 50% z-thickness for $\chi = 0$ with Cartesian mesh.

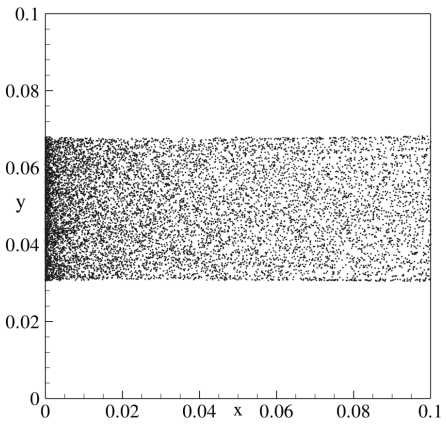

Figure 8: Particles for Cartesian mesh at 50 [ns] with $\chi = 0$.

Figure 7 shows the situation for the Cartesian mesh at simulation time $t = 50$ [ns] without divergence cleaning, only using the hyperbolic evolution equations (1) and (2).

[1]One macro particle imitates the presence of a certain number of real particles. This number is the macro particle factor.

Strong gradients of the E_x-field in the region of the electron beam indicate large charge conservation errors. Figure 8 shows the corresponding position of the particles. A weak bunching of the beam in the left part of the figure can be observed. Filaments of particles, specially on the edges of the beam, can be found in the right part of the figure. These filaments are a typical sign for inconsistencies between the electrical field and the charge density, i.e. a violation of Gauss' law (4).

In Figure 9 and 10 we find the situation for $t = 50$ [ns] with $\chi = 1$. Here we can see a smooth electrical field without strong gradients and no significant divergence errors. The particle beam is diverging and filaments, especially on the edges, are not occurring. Moreover, a more homogeneous particle distribution can be found.

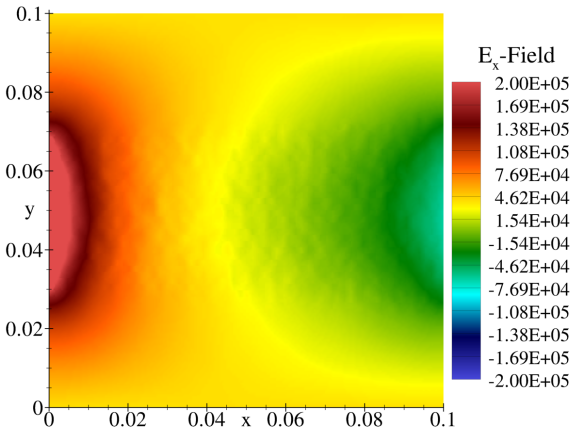

Figure 9: E_x-field at 50 [ns] of y-x-plane slice at 50% z-thickness for $\chi = 1$ with Cartesian mesh.

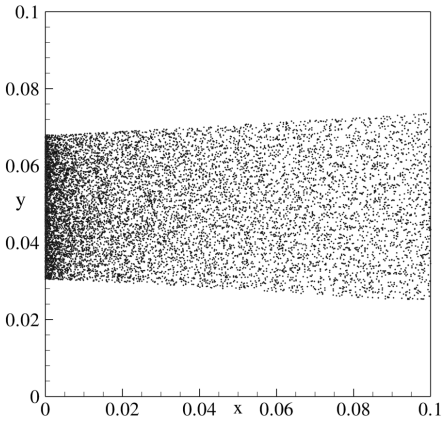

Figure 10: Particles for Cartesian mesh at 50 [ns] with $\chi = 1$.

The results for the unstructured mesh without divergence cleaning can be found in Figure 11 showing the E_x field and Figure 12 showing the corresponding particles at $t = 50$ [ns]. Strong scattering in the E_x-field indicates large charge conservation errors. The particles are totally scattered in a strong diverging fashion along the diode, which can be explained by the violation of the charge conservation. For $\chi = 1$ the results for the unstructured mesh are very similar to the results of the Cartesian mesh shown in Figure 9 and 10.

Figure 13 shows the charge conservation error for $\chi = [0, 1]$ in logarithmic scale due to a strong growth in the error with $\chi = 0$. We can find that for the unstructured grid the error grows significantly stronger than for the Cartesian grid. This can be explained by the propagation direction of the particles and the electromagnetic waves. While the Cartesian mesh is aligned with the propagation direction the unstructured mesh is not aligned. This leads to stronger errors.

Figure 14 shows the charge conservation error for the structured and unstructured grid with $\chi = [1, 2, 5]$. The errors evolve about linearly in the beginning phase and remain constant after 1.5 [ns]. Electrons are initially emitted from the left traveling about 1 [ns]

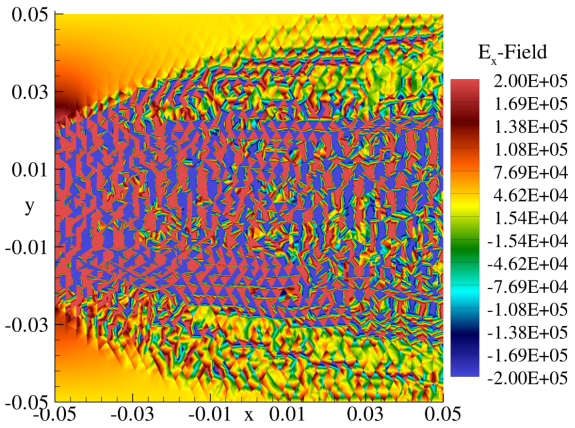

Figure 11: E_x-field at 50[ns] of y-x-plane slice at 50% z-thickness for $\chi = 0$ with unstructured mesh.

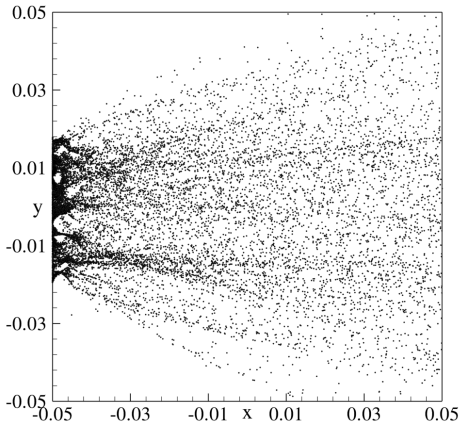

Figure 12: Particles for unstructured mesh at 50[ns] with $\chi = 0$.

to the right. After the initial phase and another 0.5 [ns] the current is fully developed and the errors stay constant. For increasing χ the error decreases as expected. Again the unstructured mesh has larger errors than the Cartesian mesh, which can be explained as mentioned above.

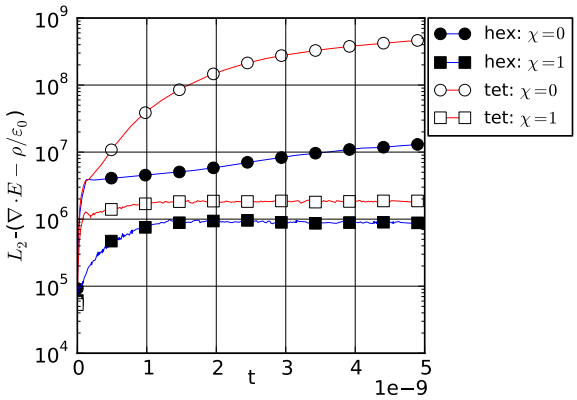

Figure 13: L_2-norm of the charge conservation error for the Cartesian and unstructured mesh using hexahedral and tetrahedral elements, respectively. Computed with the PHM8 system for $\chi = [0, 1]$.

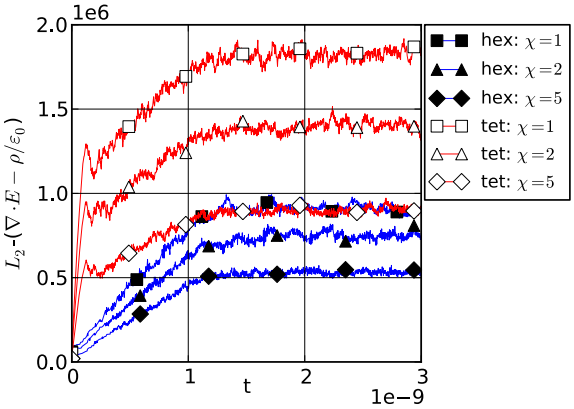

Figure 14: L_2-norm of the charge conservation error for the Cartesian and unstructured mesh using hexahedral and tetrahedral elements, respectively. Computed with the PHM8 system for $\chi = [1, 2, 5]$.

Performance tests with seven runs revealed a small speed up of the PHM7 system with a mean value of 0.021 and a standard deviation of 0.035. This is not the expected speed up of ≈ 10 %. Apparently, for a complex three-dimensional DG code on a modern cache-based CPU, it does not matter whether we use a seven or eight variable system. Latencies, caching and prefetching of data from the memory seem to have a greater effect than the computational overhead of one additional variable.

3 Conclusions

The necessity for divergence cleaning of the Maxwell equations has been demonstrated. Both test cases revealed no significant differences in the charge conservation error for both the PHM7 and PHM8 system. A significant difference exists for the enforcing of the magnetic divergence constraint. For the PHM7 system the magnetic divergence is increasing and influencing the results of electromagnetic wave propagation on a long time scale. On the short scale these errors do not influence the overall errors as shown in the pure Maxwell equations example. For an example where magnetic fields play an important role, such as the Weibel instability, this issue has to be taken into account.

A major influence on the errors is caused by the grid. In both examples the unstructured grid led to larger errors than the Cartesian grid. While for the PIC example significantly larger errors were observed, for the pure Maxwell equation example only slightly bigger errors appeared. When the grid is uniform with the wave and source propagation directions, errors are smaller than for a non-uniform grid. With $\chi = 1$ satisfactory results are achieved for both Cartesian and unstructured grids. None the less, a proper study of the wave propagation directions seems to be an important issue. A grid designed for these specific demands can improve the charge conservation and reduce magnetic divergence errors drastically and is better than using a high χ. Using high values of χ additionally is not advisable since the time step decreases due to the CFL condition leading to longer computation times.

Performance tests revealed no significant speed up for the PHM7 system compared to the PHM8 system. But memory reductions of about 1.5 % for the PHM7 system were measured. Apparently, for a complex three-dimensional DG code on a modern cache-based CPU, it does not matter whether we use a seven or eight variable system. Latencies, caching and prefetching of data from the memory seem to have a greater effect than the computational overhead of one additional variable. Thus performance considerations are not relevant for the choice of the system since the differences between them w.r.t. this issue are negligible.

In general we suggest to choose the PHM8 system since on long time scales not only the violation of charge conservation has to be considered, but also the harm of the magnetic divergence constraint, which affects the Poynting vector as well. While the PHM7 system neglects the magnetic divergence constraint the PHM8 system enforces this constraint.

4 Acknowledgement

We gratefully acknowledge the Deutsche Forschungsgemeinschaft (DFG) for funding this research within the project “Numerical Modeling and Simulation of Highly Rarefied Plasma Flows“.

REFERENCES

[1] C. Altmann, G. Gassner, F. Lörcher and C.-D. Munz, *A Space-Time Expansion Discontinuous Galerkin Scheme With Local Time Stepping for the Ideal and Viscous*

MHD Equations, IEEE Transactions on Plasma Science, 2009, Vol. 37, 513 - 519.

[2] F. Assous and P. Degond and E. Heintze and P.-A. Raviart and J. Segre, *On a finite-element method for solving the three-dimensional Maxwell equations*, J. Comput. Phys., 1993, Vol. 109, 222 - 237.

[3] Birdsall, C.K. and Langdon, A.B., *Plasma Physics via Computer Simulation*, Adam Hilger, Bristol, Philadelphia, New York, 1991.

[4] Boris, J. P., *Relativistic Plasma Simulations – Optimization of a Hybrid Code*, Proc. 4th Conf. on Num. Sim. of Plasmas, 1970, NRL Washington, Wash. DC, p. 3 - 67.

[5] A. Dedner and F. Kemm and D. Kröner and C.-D. Munz and T. Schnitzer and M. Wesenberg, *Hyperbolic divergence cleaning for the MHD equations*, J. Comput. Phys., 2001, Vol. 175, p. 645 - 673.

[6] G. Gassner and F. Lörcher and C.-D. Munz and J. S. Hesthaven, *Polymorphic Nodal Elements and their Application in Discontinuous Galerkin Methods*, J. Comput. Phys., 2009, Vol. 228, p. 1573 - 1590.

[7] J. S. Hesthaven and T. Warburton, *Nodal Discontinuous Galerkin Methods*, 2008, Springer, New York.

[8] Issautier, D. and Poupaud, F. and Cioni, J.P. and Frezoui, L., *A 2D Vlasov-Maxwell solver on unstructured meshes*, in: Proc. 3rd Intl. Conf. on Math. & Num. Aspects on Wave Prop.; G. Cohen, P.Joly, E. Becache, J.E. Roberts (eds), 1995, p. 355 - 371.

[9] Jacobs, G.B. and Hesthaven, J.S., *High-order nodal discontinuous Galerkin particle-in-cell method on unstructured grids*, J. Comput. Phys., 2006, Vol. 214, p. 96- 121.

[10] Christopher A. Kennedy and Mark H. Carpenter and R. Michael Lewis, *Low-storage, explicit Runge-Kutta schemes for the compressible Navier-Stokes equations*, Appl. Num. Math., 2000, Vol. 35, p. 177 - 219.

[11] B. Marder, *A method for incorporating Gauss' law into electromagnetic PIC codes*, J. Comput. Phy., 1987, Vol. 68, p. 48 - 55.

[12] Munz, C.-D. and Omnes, P. and Schneider, R. and Sonnendrücker, E. and Voß, U., *Divergence correction techniques for Maxwell solvers based on a hyperbolic model*. J. Comput. Phys., 2000, Vol. 161, p. 484 - 511.

[13] Munz, C.-D. and Omnes, P. and Schneider, R., *A three-dimensional finite-volume solver for the Maxwell equations with divergence cleaning on unstructured meshes*. Computer Physics Communications, 2000, Vol. 130, p. 83 - 117.